

# Ocular and uteroplacental pathology

## in macaque congenital Zika virus infection

1  
2  
3  
4  
5 Emma L. Mohr<sup>1</sup>†, Lindsey N. Block<sup>2</sup>†, Christina M. Newman<sup>2</sup>†, Laurel M. Stewart<sup>2</sup>, Michelle  
6 Koenig<sup>2</sup>, Matthew Semler<sup>2</sup>, Meghan E. Breitbach<sup>2</sup>, Leandro B. C. Teixeira<sup>3</sup>, Xiankun Zeng<sup>4</sup>, Andrea  
7 M. Weiler<sup>5</sup>, Gabrielle L. Barry<sup>5</sup>, Troy H. Thoong<sup>5</sup>, Gregory J. Wiepz<sup>5</sup>, Dawn M. Dudley<sup>2</sup>, Heather A.  
8 Simmons<sup>5</sup>, Andres Mejia<sup>5</sup>, Terry K. Morgan<sup>6</sup>, M. Shahriar Salamat<sup>2</sup>, Sarah Kohn<sup>9</sup>, Kathleen M.  
9 Antony<sup>7</sup>, Matthew T. Aliota<sup>3</sup>, Mariel S. Mohns<sup>2</sup>, Jennifer M. Hayes<sup>5</sup>, Nancy Schultz-Darken<sup>5</sup>,  
10 Michele L. Schotzko<sup>5</sup>, Eric Peterson<sup>5</sup>, Saverio Capuano III<sup>5</sup>, Jorge E. Osorio<sup>3</sup>, Shelby L. O'Connor<sup>2</sup>,  
11 Thomas C. Friedrich<sup>3,5</sup>, David H. O'Connor<sup>2,5</sup>, and Thaddeus G. Golos<sup>5,7,8</sup>.

12

13 †These authors contributed equally to this work.

14

15 \*Correspondence and request for materials should be addressed to E.L.M.

16 ([emohr@uwhealth.org](mailto:emohr@uwhealth.org)) or T.G.G. (email: [golos@primate.wisc.edu](mailto:golos@primate.wisc.edu))

17

18 Affiliations:

19 <sup>1</sup>Department of Pediatrics, University of Wisconsin-Madison

20 <sup>2</sup>Department of Pathology and Laboratory Medicine, University of Wisconsin-Madison

21 <sup>3</sup>Department of Pathobiological Sciences, University of Wisconsin-Madison

22 <sup>4</sup> United States Army Medical Research Institute of Infectious Diseases, Fort Detrick, Frederick,  
23 Maryland

24 <sup>5</sup>Wisconsin National Primate Research Center, University of Wisconsin-Madison

25 <sup>6</sup>Departments of Pathology and Obstetrics & Gynecology, Oregon Health & Science University

26 <sup>7</sup>Department of Obstetrics and Gynecology, University of Wisconsin-Madison

27 <sup>8</sup>Department of Comparative Biosciences, University of Wisconsin-Madison

28 <sup>9</sup>Department of Radiology, University of Wisconsin-Madison

29

30

## 31 **Abstract**

32 Congenital Zika virus (ZIKV) infection impacts fetal development and pregnancy outcomes. We  
33 infected a pregnant rhesus macaque with a Puerto Rican ZIKV isolate in the first trimester. The  
34 pregnancy was complicated by preterm premature rupture of membranes (PPROM) and fetal  
35 demise 49 days post infection (gestational day 95). Significant pathology at the maternal-fetal  
36 interface included acute chorioamnionitis, placental infarcts, and leukocytoclastic vasculitis of the  
37 myometrial radial arteries. ZIKV RNA was disseminated throughout the fetus tissues and  
38 maternal immune system at necropsy, as assessed by quantitative RT-PCR for viral RNA.  
39 Replicating ZIKV was identified in fetal tissues, maternal lymph node, and maternal spleen by  
40 fluorescent in situ hybridization for viral replication intermediates. Fetal ocular pathology included  
41 a choroidal coloboma, suspected anterior segment dysgenesis, and a dysplastic retina. This is  
42 the first report of ocular pathology and prolonged viral replication in both maternal and fetal  
43 tissues following congenital ZIKV infection in rhesus macaques. PPRM followed by fetal  
44 demise and severe pathology of the visual system have not been described in macaque  
45 congenital infection previously; further nonhuman primate studies are needed to determine if an  
46 increased risk for PPRM is associated with congenital Zika virus infection.

47

## 48 **Author summary**

49 A ZIKV infection during pregnancy is associated with malformations in fetal development  
50 including, but not limited to, ocular and brain anomalies, such as microcephaly, and stillbirth. The

51 development of an accurate pregnancy model to study the effects of ZIKV will provide insight into  
52 vertical transmission, ZIKV tissue distribution, and fetal injury and malformations. Non-human  
53 primates closely resemble human in terms of the reproductive system, immunity, placentation  
54 and pregnancy. Our study demonstrates that the rhesus macaque is a compelling model in which  
55 to study ZIKV during pregnancy due to similar outcomes between the human and rhesus  
56 macaque. These similarities include prolonged viremia, vertical transmission, adverse pregnancy  
57 outcomes and fetal pathology, including defects in the visual system.

58

## 59 **Introduction**

60 First isolated from a febrile rhesus macaque in Uganda in 1947, Zika virus (ZIKV) generally did  
61 not result in recognized widespread clinical disease in subsequent outbreaks across Asia and  
62 the South Pacific, until late 2015, when clinicians in Northeast Brazil reported a surge in babies  
63 born with severe birth defects (1). By early 2016, the US Centers for Disease Control and  
64 Prevention (CDC) asserted that there was a causal relationship between prenatal ZIKV infection  
65 and serious brain anomalies including microcephaly (2). The constellation of fetal and neonatal  
66 abnormalities and birth defects associated with ZIKV infection *in utero* is designated congenital  
67 Zika syndrome (CZS) (3-9). Characteristics of CZS include ocular anomalies, brain anomalies,  
68 stillbirth, cranial dysmorphologies, musculoskeletal contractures and neurologic sequelae (10).  
69 Infection during the first trimester increases the risk for birth defects (5) because critical cell  
70 proliferation and differentiation occurs during this trimester (11). One striking characteristic of  
71 CZS is a high frequency of ocular malformations, observed in as many as 55% of infants with  
72 evidence of congenital ZIKV infection and microcephaly (12, 13). Multiple case reports and case  
73 series have identified infants with ocular anomalies, which include macular pigment mottling,  
74 optic nerve hypoplasia, chorioretinal and iris coloboma, lens subluxation, retinal vascular  
75 abnormalities, cataracts and maculopathy (5, 14-21). Specific retinal defects include retinal

76 thinning, discontinuity of the retinal pigment epithelium, and colobomatous-like excavation in the  
77 neurosensory retina, retinal pigment epithelium and choroid in multiple infants (17). Because the  
78 retina develops as an outpocketing from the neural tube (22), the presence of retinal lesions  
79 implies CNS damage even without brain abnormalities.

80

81 Other recognized outcomes of congenital ZIKV infection are miscarriage, stillbirth and PPROM  
82 (23-26). The etiology of PPROM is multifactorial (27). Prenatal ZIKV infection in the first  
83 trimester of gestation results in up to 25% of pregnancies with miscarriage, fetal loss or stillbirth,  
84 with lower frequencies in the second and third trimesters in a study including 125 pregnancies  
85 (28). The CDC reports 15 fetal demise cases with birth defects out of 4,695 live births in women  
86 with confirmed ZIKV infection (29). However, this number likely does not capture the total  
87 number of fetal demises following congenital ZIKV infection because it does not include fetuses  
88 without overt birth defects even though there may be vertical transmission, or early pregnancy  
89 losses from women who were not aware of infection, or never sought a diagnosis. The  
90 pathophysiology of preterm birth or fetal loss before viability following congenital ZIKV infection  
91 has not been defined. In murine models, pregnancy following a systemic viral infection can result  
92 in an ascending bacterial uterine infection, inflammation, and preterm birth (30). It has also been  
93 reported that viral persistence of ZIKV in the lower female genital tract in the rhesus monkey is  
94 prolonged in animals treated with Depo-Provera, a synthetic progestogen (31). The specific  
95 etiology of adverse pregnancy outcomes in congenital ZIKV infection, however, is yet to be  
96 defined and requires further study.

97

98 One novel feature of ZIKV infection is the persistence of both ZIKV RNA (32-37) and replication  
99 competent virus in body fluids (33, 38) for weeks after infection. ZIKV RNA has been identified in  
100 semen between 3-188 days after infection (39, 40) with a median of 34 days (32), in urine up to  
101 29 days after infection (41) with a median of 8 days (32), in saliva up to 29 days after infection

102 (41), and in serum with a median of 14 days (32). Both ZIKV RNA and infectious particles have  
103 been isolated from breast milk 2 days after infection (42). In comparison, RNA from dengue virus  
104 (DENV), the flavivirus most closely related to ZIKV, has only been isolated from urine up to 3-4  
105 weeks after infection (43); no DENV RNA has been isolated from semen, prolonged plasma  
106 viremia has only been reported in hematopoietic stem cell recipients (44, 45), and only DENV  
107 RNA has been isolated from breast milk around the time of acute infection (46).

108 Defining the body fluid and tissue persistence of ZIKV is critical to the development of public  
109 health recommendations and solid organ and hematopoietic stem cell transplant guidelines.

110 Non-human primate (NHP) models have begun to define the tissue distribution of ZIKV following  
111 infection because defining tissue distribution in humans is not possible. Following ZIKV infection  
112 in nonpregnant NHPs, ZIKV has been identified in multiple tissues up to 35 days after infection,  
113 including the brain, spinal cord, eye, spleen, lymph nodes, muscles and joints (47, 48) and in  
114 cerebrospinal fluid (CSF) up to 42 days after infection (48), suggesting that one of these tissues  
115 may support prolonged ZIKV replication. Since prolonged ZIKV viremia is a feature of ZIKV  
116 infection during pregnancy, we hypothesized that ZIKV tissue persistence would be longer in  
117 pregnant NHPs compared to nonpregnant NHPs. Indeed, following ZIKV infection in pregnant  
118 NHPs, ZIKV RNA detection in plasma is prolonged (47) and can be detected up to 70 days after  
119 infection (49), far longer than the plasma viremia duration reported for nonpregnant NHPs (48,  
120 50).

121  
122 NHP models of both congenital infection and tissue distribution following ZIKV infection provide  
123 insight into the pathophysiology of ZIKV infection not possible through epidemiological and  
124 clinical human studies. As with humans, the rhesus macaque placenta has a hemochorial  
125 placentation with extensive endovascular invasion of the maternal endometrial spiral arterioles  
126 and arteries and innate immune cellular populations homologous with that found in the human  
127 decidua (51-53). There are multiple similarities between human and NHP ZIKV infection natural

128 history, including the duration of viremia and viruria (47, 48, 50, 54), robust neutralizing antibody  
129 responses (47, 50, 54, 55), vertical transmission (49), and fetal pathology (49, 56). To define the  
130 tissue distribution of ZIKV and fetal pathology following infection with a clinically relevant Puerto  
131 Rican isolate of ZIKV, we infected a pregnant rhesus macaque in the first trimester and  
132 performed a necropsy of the dam and fetus to comprehensively define maternal and fetal viral  
133 tissue distribution following spontaneous fetal death 49 days post-infection. Here, we describe  
134 the pregnancy outcome, maternal and fetal viral tissue distribution, and fetal pathology  
135 associated with first trimester ZIKV infection in a case of fetal demise.

136

## 137 **Materials & Methods**

138

### 139 Study Design

140 A 3.8 year old, primigravida rhesus macaque (*Macaca mulatta*) of Indian ancestry was infected  
141 subcutaneously with  $1 \times 10^4$  PFU Zika virus/H.sapiens-tc/PUR/2015/PRVABC59\_v3c2  
142 (PRVABC59) during the first trimester, 46 days gestation (term  $165 \pm 10$  days). This macaque was  
143 part of the Specific Pathogen Free (SPF) colony at the Wisconsin National Primate Research  
144 Center (WNPRC) and was free of Macacine herpesvirus 1 (Herpes B), Simian Retrovirus Type D  
145 (SRV), Simian T-lymphotropic virus Type 1 (STLV), and Simian Immunodeficiency Virus (SIV).

146

### 147 Ethics

148 All monkeys are cared for by the staff at the WNPRC in accordance with the regulations and  
149 guidelines outlined in the Animal Welfare Act and the Guide for the Care and Use of Laboratory  
150 Animals and the recommendations of the Weatherall report ([https://royalsociety.org/topics-](https://royalsociety.org/topics-policy/publications/2006/weatherall-report/)  
151 [policy/publications/2006/weatherall-report/](https://royalsociety.org/topics-policy/publications/2006/weatherall-report/)). This study was approved by the University of

152 Wisconsin-Madison Graduate School Institutional Animal Care and Use Committee (animal  
153 protocol number G005401).

154

155 Care & Use of Macaques

156 The female monkey described in this report was co-housed with a compatible male and  
157 observed daily for menses and breeding. Pregnancy was detected by ultrasound examination of  
158 the uterus at approximately 20-24 gestation days (gd) following the predicted day of ovulation.

159 The gd was estimated (+/- 2 days) based on the dam's menstrual cycle, observation of  
160 copulation, and the greatest length of the fetus at initial ultrasound examination which was  
161 compared to normative growth data in this species (57). For physical examinations, virus  
162 inoculations, some ultrasound examinations, blood and swab collections, the dam was  
163 anesthetized with an intramuscular dose of ketamine (10 mg/kg). Blood samples from the  
164 femoral or saphenous vein were obtained using a vacutainer system or needle and syringe. The  
165 pregnant macaque was monitored daily prior to and after inoculation for any clinical signs of  
166 infection (e.g., diarrhea, inappetence, inactivity and atypical behaviors). This macaque developed  
167 chronic diarrhea prior to conception and was treated daily with oral tylosin throughout pregnancy.

168

169 Inoculation and monitoring

170 ZIKV strain PRVABC59 (GenBank: KU501215), originally isolated from a traveler to Puerto Rico  
171 and passaged three times on Vero cells (American Type Culture Collection (ATCC): CCL-81),  
172 was obtained from Brandy Russell (CDC, Ft. Collins, CO). Virus stocks were prepared by  
173 inoculation onto a confluent monolayer of C6/36 cells (*Aedes albopictus* larval cells; ATCC: CCL-  
174 1660) with two rounds of amplification. The inoculating stock was prepared and validated as  
175 previously described (49, 50). The animal was anesthetized as described above, and 1 mL of  
176 inoculum at  $1 \times 10^4$  PFU dilution in PBS was administered subcutaneously over the cranial

177 dorsum. Post-inoculation, the animal was closely monitored by veterinary and animal care staff  
178 for adverse reactions or any signs of disease.

179

180 Pregnancy monitoring and fetal measurements

181 Weekly ultrasounds were conducted to observe the health of the fetus and to obtain  
182 measurements including fetal femur length (FL), biparietal diameter (BPD), head circumference  
183 (HC), and heart rate, with methods as previously described (49). Growth curves were developed  
184 for FL, BPD, and HC (58). Mean measurements and standard deviations at specified days of  
185 gestation in rhesus macaques were retrieved from Tarantal et al. (57) and the data were plotted  
186 against normative data for fetal rhesus macaques (58). The actual growth measurements were  
187 obtained from weekly ultrasound data and used to retrieve the predicted growth measurement by  
188 plotting the obtained experimental growth measurement against the growth curves. Data were  
189 then graphed as actual gestation age versus predicted gestation age to depict rate of growth  
190 compared to uninfected, control rhesus macaques (method described previously in (49)).

191 Doppler ultrasounds to measure fetal heart rate were performed as requested by veterinary staff.

192

193 Amniocentesis

194 For the amniocentesis procedures reported, animals were shaved, and the skin was prepped  
195 with Betadyne® solution, and sterile syringes, needles and gloves were used during the  
196 amniocentesis procedure. Under real-time ultrasound guidance, a 22 gauge, 3.5 inch Quincke  
197 spinal needle was inserted into the amniotic sac as described previously (49). The first 1.5-2 mL  
198 of fluid was discarded due to potential maternal contamination, and an additional 3-4 mL of  
199 amniotic fluid was collected in a new sterile syringe for viral qRT-PCR analysis as described  
200 elsewhere (50). These samples were obtained at the gestational ages specified in Figure 1. All  
201 fluids were free of any blood contamination.

202



203 vRNA isolation from body fluids and tissues

204 RNA was isolated from maternal plasma, urine, saliva and amniotic fluid using the Viral Total  
205 Nucleic Acid Purification Kit (Promega, Madison, WI, USA) and from maternal and fetal tissues  
206 using the Maxwell 16 LEV simplyRNA Tissue Kit (Promega, Madison, WI) on a Maxwell 16 MDx  
207 instrument as previously reported (50). Fetal and maternal tissues were processed with  
208 RNeasy® (Qiagen, Crawley, UK) according to manufacturer protocols. 20-40 mg of each  
209 tissue was homogenized using homogenization buffer from the Maxwell 16 LEV simplyRNA  
210 Tissue Kit and two 5 mm stainless steel beads (Qiagen, Hilden, Germany) in a 2 mL snap-cap  
211 tube, shaking twice for 3 minutes at 20 Hz each side in a TissueLyser (Qiagen, Hilden,  
212 Germany). The isolation was continued according to the Maxwell 16 LEV simplyRNA Tissue Kit  
213 protocol, and samples were eluted into 50 µL RNase free water.

214

215 Viral quantification by plaque assay

216 Titrations for replication competent virus quantification of amniotic fluid was completed by plaque  
217 assay on Vero cell cultures as described previously (50). Vero cells were obtained from  
218 American Type Culture Collection (CCL-81), were not further authenticated and were not  
219 specifically tested for mycoplasma. Duplicate wells were infected with 0.1 ml of aliquots from  
220 serial 10-fold dilutions in growth media and virus was adsorbed for 1 h. Following incubation, the  
221 inoculum was removed, and monolayers were overlaid with 3 ml containing a 1:1 mixture of 1.2%  
222 oxoid agar and 2 DMEM (Gibco, Carlsbad, CA, USA) with 10% (vol/vol) FBS and 2% (vol/vol)  
223 penicillin/streptomycin. Cells were incubated at 37°C in 5% CO<sub>2</sub> for 4 days for plaque  
224 development. Cell monolayers then were stained with 3 ml of overlay containing a 1:1 mixture of  
225 1.2% oxoid agar and 2 DMEM with 2% (vol/vol) FBS, 2% (vol/vol) penicillin/streptomycin and  
226 0.33% neutral red (Gibco). Cells were incubated overnight at 37°C and plaques were counted.

227

228 Plaque Reduction Neutralization test (PRNT)

229 Macaque serum samples were screened for ZIKV neutralizing antibodies utilizing a plaque  
230 reduction neutralization test (PRNT). End point titrations of reactive sera, utilizing a 90% cutoff  
231 (PRNT90), were performed as described (59) against ZIKV strain PRVABC59. Briefly, ZIKV was  
232 mixed with serial 2-fold dilutions of serum for 1 hour at 37°C prior to being added to Vero cells  
233 and neutralization curves were generated using GraphPad Prism software (La Jolla, CA). The  
234 resulting data were analyzed by nonlinear regression to estimate the dilution of serum required to  
235 inhibit both 90% and 50% of infection.

236

### 237 Maternal and neonatal necropsy

238 At 49 days post infection (dpi) (gd 95), no fetal heartbeat was detected. The dam was sedated,  
239 euthanized, and sterile instruments were used for the dissection and collection of all maternal,  
240 fetal, and maternal-fetal interface tissues during the gross post-mortem examination. Amniotic  
241 fluid was aspirated with a syringe and needle inserted through the uterine wall into the lumen.  
242 Each tissue was collected with a unique set of sterile instruments and placed in a separate sterile  
243 petri dish before transfer to appropriate containers for viral RNA analysis and histology, to  
244 prevent cross-contamination between tissues. Tissue distribution for subsequent analysis was as  
245 previously described (49).

246

### 247 Histology

248 For general pathology, tissues were fixed in 4% PFA as for IHC, routinely processed and  
249 embedded in paraffin. Paraffin sections (5 µm) were stained with hematoxylin and eosin (H&E).  
250 Two veterinary pathologists were blinded to vRNA findings when tissue sections were evaluated  
251 microscopically. Lesions in each tissue were described and assigned morphologic diagnoses as  
252 described previously (49). Photomicrographs were obtained using brightfield microscopes  
253 Olympus BX43 and Olympus BX46 (Olympus Inc., Center Valley, PA) with attached Olympus  
254 DP72 digital camera (Olympus Inc.) and Spot Flex 152 64 Mp camera (Spot Imaging, Sterling

255 Heights, MI), and captured using commercially available image-analysis software (cellSens  
256 DimensionR, Olympus Inc. and Spot software 5.3). Uteroplacental pathology was specifically  
257 performed by an experienced placental pathologist (T.K.M.).

258

259 In situ hybridization

260 In situ hybridization (ISH) was conducted with tissues fixed in 4% PFA, and alcohol processed  
261 and paraffin embedded, as for IHC. ISH probes against Zika genome were purchased  
262 commercially (Advanced Cell Diagnostics, Cat No. 468361, Newark, California, USA). ISH was  
263 performed using the RNAscope® Red 2.5 Kit (Advanced Cell Diagnostics, Cat No. 322350)  
264 according to the manufacturer's instructions. Briefly, after deparaffinization with xylene, a series  
265 of ethanol washes, and peroxidase blocking, sections were heated in boiling antigen retrieval  
266 buffer for 15 minutes and then digested by proteinase K (2.5 ug/ml, to completely cover the section)  
267 for 16 minutes at 40°C. Sections were exposed to ISH target probe and incubated at 40°C in a  
268 hybridization oven for 2 h. After rinsing, ISH signal was amplified using company-provided Pre-  
269 amplifier and Amplifier conjugated to horseradish peroxidase (HRP), and incubated with a red  
270 substrate-chromogen solution for 10 min at room temperature.

271

272 Multiplex fluorescent in situ hybridization

273 Multiplex fluorescent in situ hybridization (mFISH) was conducted with tissues fixed in 4% PFA  
274 as for IHC. mFISH was performed using the RNAscope® Fluorescent Multiplex Kit (Catalog #  
275 320850, Advanced Cell Diagnostics) according to the manufacturer's instructions with  
276 modifications. Probes with C1 channel (Cat# 468361, red) targeting ZIKV positive sense RNA  
277 and probes with C3 channel (Cat# 467911, green) targeting ZIKV negative sense RNA were  
278 synthesized by Advanced Cell Diagnostics. Paraformaldehyde fixed paraffin embedded rhesus  
279 monkey fetus tissue sections underwent deparaffinization with xylene and a series of ethanol  
280 washes. These tissue sections were treated with 0.1% Sudan Black B (Sigma-Aldrich, St. Louis,

281 MO, USA) to reduce autofluorescence, heated in antigen retrieval buffer (Citrate buffer with pH  
282 6.0), and digested by proteinase. Sections were exposed to ISH target probes and incubated at  
283 40°C in a hybridization oven for 2 h. After rinsing, ISH signal was amplified using company-  
284 provided Pre-amplifier and Amplifier conjugated to fluorescent dye. Sections were counterstained  
285 with 4', 6-diamidino-2-phenylindole (DAPI, Thermo Fisher Scientific, Waltham, MA, USA),  
286 mounted, and stored at 4°C until image analysis. mFISH images were captured on an LSM 880  
287 Confocal Microscope with Airyscan (Zeiss, Oberkochen, Germany) and processed using open-  
288 source ImageJ software (National Institutes of Health, Bethesda, MD, USA).

289

290 Placental alpha microglobulin-1 (PAMG-1) immunochromatographic assay

291 A PAMG-1 immunochromatographic assay (AmniSure<sup>®</sup> ROM (Rupture of [fetal] Membranes)

292 test, Qiagen, Boston, MA, FMRT-1-10-US) was performed according to the manufacturer's

293 protocol with urine and amniotic fluid samples that had been stored at -80°C. A sterile polyester

294 swab, provided by the manufacturer, was inserted into a tube containing the sample fluid for 1

295 minute. The swab was then added to the solvent microfuge tube and rotated by hand for 1

296 minute. Finally, the test strip was placed into the solvent and incubated at room temperature for

297 10 minutes before the test strip was read and photographs were taken. A term amniotic fluid

298 sample was the positive control and non-pregnant urine was the negative control. Open-source

299 ImageJ software was used to measure the relative pixel density of each band (control and test

300 band) (National Institutes of Health, Bethesda, MD, USA). The pixel density of each band was

301 measured, the background density was subtracted, and the relative pixel density of each test

302 band was calculated by subtracting the control band density from the test band density.

303

304 Insulin-like growth factor-binding protein 1 (IGFBP-1) ELISA

305 An IGFBP-1 ELISA kit (Abcam, Cambridge, MA, ab100539) was used to determine if a marker

306 for amniotic fluid was detectable in maternal urine. The protocol was followed as specified by the

307 manufacturer and all samples were frozen undiluted at -80°C until use. Duplicates were run for  
308 the standards, samples, positive, and negative controls. A term amniotic fluid sample was used  
309 as the positive control and male urine and non-pregnant female urine were used as negative  
310 controls. All urines were diluted 1:5000 and all amniotic fluid samples were diluted 1:20,000.  
311 Immediately upon addition of the stop solution the plate was read at 450 nm. A standard curve  
312 was calculated from the average of each standard. This standard curve equation was used to  
313 calculate the concentration of each sample.

314

315 Data availability

316 Primary data that support the findings of this study are available at the Zika Open-Research  
317 Portal (<https://zika.labkey.com/project/OConnor/ZIKV-019/begin.view?>). Zika virus/H.sapiens-  
318 tc/PUR/2015/PRVABC59-v3c2 sequence data have been deposited in the Sequence Read  
319 Archive (SRA) with accession code SRX2975259. The authors declare that all other data  
320 supporting the findings of this study are available within the article and its supplementary  
321 information files.

322

## 323 **Results**

324

325 Pregnancy outcome

326 A pregnant rhesus macaque was subcutaneously inoculated with  $1 \times 10^4$  PFU ZIKV-Puerto Rico  
327 at gd46. She had no fever, rash, or inappetence detected following inoculation. The pregnancy  
328 was monitored by ultrasonography, vRNA titers in blood, and urine samples, and neutralizing  
329 antibody titers at multiple times throughout pregnancy; amniotic fluid and maternal CSF were  
330 collected at several time points (Figure 1).

331

332 Maternal plasma viremia was detected from days 1 through 18 post-infection, peaking at 5 dpi  
333 with  $2.55 \times 10^5$  vRNA copies per mL, and was also detected at 24 dpi (Figure 2). At 21 dpi the  
334 viral load dropped below 100 vRNA copies per mL, the limit of quantification of the qRT-PCR  
335 assay. Amniotic fluid at 28 dpi had a viral load of  $1.84 \times 10^4$  vRNA copies per mL. The amniotic  
336 fluid was reported as clear, and a plaque assay performed on the amniotic fluid was negative  
337 (data not shown). Saliva samples remained negative throughout pregnancy (data not shown).  
338 CSF samples taken at 7, 14, and 49 dpi were all negative. ZIKV RNA was first detected in a  
339 passively collected urine sample (i.e. in pan at the bottom of the cage) at 42 dpi, with a  
340 concentration of  $7 \times 10^4$  vRNA copies per mL, and was present in the urine until euthanasia at 49  
341 dpi.

342  
343 In addition to vRNA in body fluids, the development of maternal ZIKV-specific antibodies was  
344 assessed. Plaque reduction neutralization tests (PRNT) were performed on serum collected at  
345 10, 28, and 49 dpi. All post-infection time points demonstrated the presence of ZIKV-specific  
346 neutralizing antibodies with an increasing concentration of neutralizing antibodies throughout the  
347 post-infection period (Figure 3).

348  
349 Because identifying urine vRNA so long after infection was unexpected, and its presence  
350 coincided with the presence of vRNA in the amniotic fluid, we wanted to determine whether the  
351 passively collected urine contained amniotic fluid, a potential harbinger of an adverse pregnancy  
352 outcome. We performed an AmniSure<sup>®</sup> test, which detects an amniotic fluid protein, placental  
353 alpha microglobulin-1, (PAMG-1), and determined that urine contained detectable PAMG-1  
354 (Figure 4). As expected, the 28 dpi amniotic fluid was positive for PAMG-1, as was the positive  
355 control term amniotic fluid from a different animal. The 28 dpi urine (collected just prior to the  
356 amniocentesis) was negative for PAMG-1, however the 45 and 49 dpi urine samples were  
357 positive for PAMG-1. The negative control was a non-pregnant urine sample. AmniSure<sup>®</sup> is not a

358 quantitative test but the result suggested there was amniotic fluid in the urine samples at 45 and  
359 49 dpi. To confirm this finding, we performed an insulin-like growth factor binding protein-1  
360 (IGFBP-1) ELISA on the animal's pan-collected urine and amniotic fluid samples, along with  
361 appropriate controls. IGFBP-1 is a 25 kD protein synthesized and secreted by the fetal liver and  
362 maternal decidua, and is present in amniotic fluid from the second trimester of pregnancy until  
363 full term (60). It is not found in urine. In the pregnant animal, IGFBP-1 was detected in pan-  
364 collected urine at levels similar to that in amniotic fluid alone, confirming the presence of amniotic  
365 fluid-specific protein in the urine (Figure 4). The IGFBP-1 levels in urine from this dam were  
366 higher than negative control urine samples (urine from a male and a nonpregnant female) but  
367 lower than amniotic fluid from a control macaque late in gestation, which is consistent with  
368 dilution from urine from passive collection. Thus, the presence of amniotic fluid in the urine is  
369 consistent with premature rupture of membranes.

370

### 371 Ultrasonography

372 The fetus displayed typical growth in all parameters when compared with normative data (Figure  
373 5) (58). Plotting the predicted gestational age (pGA) vs. the clinically estimated (actual)  
374 gestational age (aGA) can reveal changes in the trajectory of a specific growth parameter (49,  
375 57); this analysis did not reveal any growth trajectory anomalies (Figure 5B growth chart).

376

377 We also closely observed placental and fetal health by ultrasonography. No significant placental  
378 lesions were identified until 35 dpi (gd 81) when ultrasonography identified a possible area of  
379 placental abruption and a retroplacental clot along the edge of the placenta over the cervix,  
380 which was resolving by 42 dpi (gd 88). No fetal abnormalities were noted at either time point, and  
381 the fetus did not demonstrate any persistent tachycardia or bradycardia. Because of these small  
382 placental lesions, daily heart rate monitoring was initiated and remained within a normal range  
383 until 49 dpi (gd 95) when no fetal heartbeat was detected.

384

385 The dam underwent euthanasia and necropsy for a comprehensive collection of both maternal  
386 and fetal tissues. During the necropsy, the cervix was noted to be closed and no debris was  
387 noted in the vaginal vault. The amniotic sac contained significant amounts of adherent purulent  
388 matter, and purulent fibrinous material covered the decidua and fetus (Figure 6). The fetus  
389 showed advanced tissue autolysis, including severe autolysis of the fetal brain (not shown).  
390 Bacterial culture obtained by swab of the fibrinopurulent amniotic fluid at the time of necropsy  
391 demonstrated *Staphylococcus epidermidis*. We also identified clusters of gram positive cocci in  
392 the fetal esophageal lumen (Supplementary Figure 1). *S. epidermidis* is part of the vaginal flora  
393 in rhesus macaques (61). No additional samples were obtained for culture or bacterial 16s rDNA-  
394 PCR.

395

396 Fetal and maternal vRNA tissue distribution

397 At necropsy, a range of fetal and maternal tissues were processed for qRT-PCR to determine  
398 ZIKV RNA burden. ZIKV RNA was widely distributed within fetal tissues, maternal lymphoid  
399 structures, and the reproductive tract: 33 fetal, maternal and maternal-fetal interface tissues were  
400 positive for vRNA (Table 1 vRNA); of these, 27 were fetal tissues. Amniotic fluid collected during  
401 necropsy also contained vRNA (Figure 2) but did not contain replicating virus as assessed via  
402 plaque assay (not shown). The highest viral loads were detected in fetal colon and fetal lung  
403 tissue. Most organs of the fetal digestive system had detectable vRNA: stomach, jejunum, and  
404 colon. The presence of vRNA in fetal ocular structures and cerebellum indicates a central  
405 nervous system infection. vRNA was detected in four maternal lymph nodes and the spleen,  
406 indicating that ZIKV RNA was still present in the maternal immune system structures at 49 dpi,  
407 despite the absence of detectable maternal viremia.

408

409 Table 1: Tissues with detectable ZIKV RNA from mother and fetus



| Tissue Source   | Organ System | Tissue Name                 | vRNA copies/mg |
|-----------------|--------------|-----------------------------|----------------|
| Maternal        | Immune       | Axillary LN                 | 258.3          |
|                 |              | Inguinal LN                 | 1774.8         |
|                 |              | Mesenteric LN               | 9763.8         |
|                 |              | Spleen                      | 981.9          |
|                 |              | Pelvic LN                   | 583.7          |
|                 | Reproductive | Decidua                     | 278.2          |
|                 |              | Uterus                      | 1471.7         |
|                 |              | Uterus/placental bed        | 486.5          |
|                 | Fetal        | Alimentary Canal            | Stomach        |
| Colon           |              |                             | 355157         |
| Jejunum         |              |                             | 2055.9         |
| Liver           |              |                             | 5.4            |
| Renal           |              | Kidneys                     | 51.1           |
|                 |              | Urinary Bladder             | 185.1          |
| Cardiovascular  |              | Aorta-thoracic              | 921.3          |
|                 |              | Heart                       | 366            |
|                 |              | Pericardium                 | 1196.3         |
| Extraembryonic  |              | Amniotic Chorionic Membrane | 4933.7         |
|                 |              | Placental Disc 1            | 64.4           |
|                 |              | Umbilical Cord              | 6              |
| Connective      |              | Adipose Tissue-Omentum      | 5102.2         |
| Immune          |              | Axillary LN                 | 287.6          |
|                 |              | Spleen                      | 261.1          |
|                 |              | Thymus                      | 215.3          |
| Musculoskeletal |              | Muscle-quadriceps           | 387            |
| Pulmonary       |              | Lung                        | 37947          |
| Reproductive    |              | Sem vesicle/Prostate        | 5700           |
|                 |              | Testis                      | 5188.1         |
| Central Nervous |              | Cerebrum                    | 72.9           |
|                 |              | Dura Mater                  | 74.3           |
| Ocular          |              | Cornea                      | 135.1          |
|                 |              | Retina                      | 316.5          |
|                 |              | Sclera                      | 370.8          |

410  
411 127 maternal biopsies and fetal tissues were assayed for vRNA. All the tissues positive for ZIKV  
412 RNA are listed in this table. The maternal and fetal tissues which were vRNA negative are listed  
413 in Supplementary Table 1.

414

#### 415 Uteroplacental histopathology

416 Maternal-fetal interface tissues were evaluated for histological evidence of infection and lesions.

417 There was clear evidence of both acute chorioamnionitis consistent with bacterial infection

418 (Figure 7A), and features of relative placental insufficiency. There is no acute or chronic villitis,

419 but the villi do show increased perivillous fibrin deposition (Figure 7B), and there are multiple

420 remote infarctions (Figure 7C), which is a finding consistent with insufficiency. Radial arteries in

421 the myometrium showed a pronounced leukocytoclastic vasculitis defined as an infiltrative

422 mixture of lymphocytes, eosinophils, and plasma cells into the smooth muscle wall of these

423 vessels (Figure 7D). The leukocytoclastic vasculitis seen around the radial arteries is usually

424 related to hypersensitivity reactions or viral infections, and is not a consequence of bacterial

425 infection. The decidua, placenta, placental bed and amniotic/chorionic membranes also showed

426 significant pathology (Supplementary Table 2).

427

#### 428 Fetal ocular histopathology

429 In our previous study (49), 2/2 macaque fetuses from first trimester ZIKV infection had

430 suppurative inflammation in the ocular tissues at term (retina, choroid, optic nerve). In the current

431 study, ocular tissues were therefore carefully evaluated by qRT-PCR and histology. One fetal

432 eye was dissected for vRNA detection by qRT-PCR and the contralateral eye was fixed and

433 processed for histological analysis. ZIKV RNA was detected by qRT-PCR in the retina, choroid,

434 and lens at low levels (TABLE 1 vRNA). At the time of demise the fetal eyelids were still fused,

435 suggesting that vRNA present in the eye was not due to passage of the virus from the amniotic

436 fluid directly across the cornea or sclera.

437

438 In the fixed and processed globe, a chorioretinal coloboma affecting the ventral aspect of the

439 globe was revealed, and was characterized by extensive areas of choroidal and scleral thinning

440 with a central area of choroidal and retinal pigmented epithelium absence and marked dysplasia  
441 of the adjacent retina (Figure 8). Additionally, the presence of fusion of the iris with the posterior  
442 corneal stroma and a seeming lack of adequate maturation of the iridocorneal angle structures  
443 suggested the presence of anterior segment dysgenesis. It is necessary to acknowledge that the  
444 histologic interpretation of the anterior segment changes in this globe was hampered by the  
445 tissue autolysis presence in the fetus. Although the chorioretinal lesions were obvious even with  
446 a mild degree of autolysis, the autolytic changes impacted our ability to analyze the delicate  
447 structure of the developing tissues of the iridocorneal angles, making it impossible to definitively  
448 diagnose anterior segment dysgenesis. Because the retina is part of the central nervous system,  
449 the finding of retinal dysplasia indicates that the fetus had CNS abnormalities. The presence of  
450 the coloboma, dysplastic retina, and potential anterior segment dysgenesis are abnormalities  
451 that likely arose from disruption of early ocular developmental processes (62), consistent with the  
452 first trimester window of sensitivity in our earlier study (49).

453

454 Tissue pathology and detection of vRNA in maternal and fetal tissues

455 Histologic lesions were noted in the fetal tissues that were potentially exposed to virus in the  
456 amniotic fluid, specifically the respiratory and gastrointestinal systems. There were significant  
457 lesions in the lungs, mesenteric lymph node, placenta, chorioamniotic membranes, decidua,  
458 maternal uterus, and maternal spleen (Supplementary Table 2). Consistent with the bacterial  
459 growth of *S. epidermidis* from amniotic fluid, gram positive cocci were observed within the lumen  
460 of the esophagus (Supplementary Figure 1), although there was no associated inflammatory  
461 reaction within the epithelium or deeper tissue layers of the esophagus. The stomach and small  
462 intestine had mucosal autolysis with no discernible histologic lesions. The lumen of the colon had  
463 granular basophilic material consistent with nuclear debris.

464

465 The fetal lungs had notable pathology. The pulmonary alveoli had fibrin, cellular debris, edema,  
 466 occasional squamous cells, and neutrophilic infiltration (alveolitis). There were multiple areas of  
 467 alveoli with type II pneumocyte hyperplasia, with multifocal expansion of the alveolar septa with  
 468 fibrin. The trachea, primary and secondary bronchi, had relatively intact respiratory epithelium.

469

470 ZIKV histological analyses

471 ZIKV RNA localization was evaluated by ISH and mFISH on selected tissues with high vRNA  
 472 burden as determined by qRT-PCR. Figure 9 presents photomicrographs from near sections of  
 473 the same spleen, fetal membranes, and fetal lung specimens. H&E staining is presented to  
 474 demonstrate tissue organization and pathology; ISH to confirm the presence of ZIKV genome  
 475 within cells, and mFISH for both negative and positive strand ZIKV RNAs to detect the dsRNA of  
 476 replicative intermediates. Supplementary Figure 2 also presents representative images of  
 477 positive and negative strand RNAs for the tissues displayed; the merged figure colocalizes both  
 478 positive and negative sense RNA strands, indicating active ZIKV replication in these tissues.

479

480 Table 2: Tissue vRNA burden, ISH and mFISH results.

| Tissue Source | Tissue Name                 | vRNA copies/mg    | ISH | mFISH |
|---------------|-----------------------------|-------------------|-----|-------|
| Maternal      | Mesenteric LN               | 976.38            | -   |       |
|               | Spleen                      | 98.19             | +   | +     |
|               | Uterus                      | 147.17            | +   | +     |
|               | Decidua                     | 27.82             | +   | +     |
|               | Amniotic/Chorionic Membrane | 493.37            | +   | +     |
|               | Colon                       | 35515.7           | +   | +     |
| Fetal         | Stomach                     | 614.04            | -   |       |
|               | Pericardium                 | 119.63            | -   |       |
|               | Adipose Tissue-Omentum      | 510.22            | +   | -     |
|               | Lung                        | 3794.70           | +   | +     |
|               | Seminal Vesicle/Prostate    | 570.00            | -   |       |
|               | Testis                      | 518.81            | -   |       |
|               | Eye (Retina/Cornea/Sclera)  | 31.65/13.51/37.08 | -   |       |

481

482

483 Tissues with a detectable vRNA burden were evaluated by ISH and mFISH. ISH detects positive  
484 sense vRNA; mFISH detects ZIKV replicative intermediates (negative and positive sense vRNA).  
485 “+” indicates detectable signal in these tissues sections, “-“ indicates no signal. Tissues with no  
486 detectable ISH signal were not further evaluated by mFISH.

487

## 488 **Discussion**

489 In this report of an adverse pregnancy outcome following ZIKV infection in a rhesus macaque,  
490 we describe fetal demise following suspected PPRM, fetal and maternal ZIKV burden, and  
491 significant ocular pathology in the fetus. ZIKV RNA was widely distributed throughout fetal  
492 tissues at necropsy, including in the cerebellum and ocular tissues. ZIKV vRNA was also  
493 identified in maternal lymph nodes and maternal spleen at the time of necropsy (49 dpi).  
494 Replication competent virus was identified by ISH for the presence of negative and positive  
495 strand RNA in fetal and maternal tissues. Abnormal histology was characterized in multiple fetal  
496 tissues including alveolitis and pneumocyte hyperplasia in fetal lung tissue, and severe ocular  
497 abnormalities. Both fetal ocular pathology and fetal demise have been described in human  
498 reports of ZIKV infection and demonstrate parallels between human and NHP CZS.

499

500 Fetal demise

501 This is the first report of rupture of membranes and fetal demise in an NHP model of congenital  
502 ZIKV infection. We presume that maternal membranes ruptured around 42 dpi (although some  
503 amniotic fluid may have been present at 28 dpi) because we detected amniotic fluid markers in  
504 the urine at this time point, and identified high vRNA burden in this urine sample, despite  
505 absence of detectable maternal viremia at this time. A week after detection of ZIKV RNA in the  
506 pan-collected urine/amniotic fluid mixture, abdominal ultrasound evaluation found no fetal  
507 heartbeat and the fetus and dam were submitted for necropsy. There was no chronic villitis,

508 which would be expected for viral induced changes. However, sections of the decidua and  
509 myometrium revealed a pronounced leukocytoclastic vasculitis involving the smooth muscle  
510 walls of the radial and spiral arteries. This is significant because this type of vasculitis is not  
511 expected in cases of bacterial infection, but do occur as a response to viral infections associated  
512 with cutaneous vasculitis (hypersensitivity vasculitis) (63).

513  
514 Although there was fibrinopurulent material surrounding the fetus in the uterine cavity and gram  
515 positive cocci in the esophagus, multiple sections of placenta and all other fetal tissues had no  
516 histologic evidence of bacterial colonization. The growth of *S. epidermidis* from aspirated  
517 amniotic fluid was minimal and contamination at the time of collection is a possibility. Neutrophilic  
518 infiltration, such as that seen in the chorionic plate, is consistent with bacterial infection, but intra-  
519 amniotic neutrophilic inflammation can also be sterile (64). Sterile neutrophilic inflammation has  
520 been reported previously in experimental infection in animals models with this strain of ZIKV,  
521 including mice which demonstrated neutrophil infiltration of the skeletal muscle and hippocampus  
522 (65) and male rhesus macaques which demonstrated interstitial neutrophilic prostatitis (47).  
523 Therefore, while this clinical presentation is consistent with an ascending bacterial intraamniotic  
524 infection, further studies will be able to provide clarification of the histopathologic outcomes with  
525 macaque pregnancies.

526  
527 Closely associated with this fetal demise is the occurrence of PPROM. Although it is not possible  
528 to determine if the amniotic membranes ruptured because of ZIKV infection, the finding of  
529 PPROM followed by fetal demise also occurs during human prenatal ZIKV infection (24). It could  
530 be hypothesized that the amniocentesis at 28 dpi contributed to the possible intrauterine  
531 bacterial infection; however, the long duration of time separating these events, and the typical  
532 rapidity of preterm labor in the rhesus macaque with experimental bacterial infection of the  
533 amniotic fluid makes this unlikely (66, 67). Additional studies of ZIKV infection during NHP

534 pregnancy are needed to determine if there is an association between congenital ZIKV infection  
535 and an increased risk for intra-amniotic infection leading to PPRM and fetal demise. One may  
536 speculate that ZIKV infection early in gestation affects pregnancy-induced T-cell changes or  
537 placental invasion involved in uterine vascular remodeling necessary for normal blood flow to the  
538 placenta. In turn, ZIKV infection may lead to abnormal remodeling and abnormal blood flow to  
539 the placenta culminating in pathologic infarctions and increased risk for relative placental  
540 insufficiency and preterm birth. This working hypothesis requires further study.

541

542 Fetal ocular defects

543 Congenital ocular abnormalities are strongly associated with human prenatal ZIKV infection, as  
544 demonstrated by the high frequency (up to 55%) of ocular disease in human infants with first  
545 trimester prenatal infections (12). There is growing evidence that structures of the fetal visual  
546 system are a significant target for ZIKV in human pregnancy. The fetal eye evaluated for  
547 pathology in the current study had anterior segment dysgenesis, a ventral choroidal coloboma,  
548 and retinal dysplasia. This is the first time that such severe ocular abnormalities have been  
549 reported with macaque CZS. As far as we are aware, bacterial infections are not associated with  
550 such abnormalities during development. In addition, an acute intrauterine bacterial infection  
551 would not have impacted eye development, since the ocular structure damage described would  
552 likely have occurred from the disruption of normal developmental processes which occur earlier  
553 in pregnancy. Anterior segment dysgenesis refers to a spectrum of developmental anomalies  
554 resulting from abnormalities of neural crest migration and differentiation during fetal development  
555 (68). In humans, anterior segment dysgenesis is present in rare syndromes (69), and although  
556 the rate of anterior segment dysgenesis and related syndromes is unknown in rhesus macaques,  
557 it would be unlikely to appear in pregnancy.

558

559 An ocular coloboma is a congenital lesion associated with a failure in the closure of the  
560 embryonic (ocular) fissure causing defects of one or more ocular structures (i.e., the eyelids,  
561 lens, cornea, iris, ciliary body, zonules, choroid, retina and optic nerve). The defect is essentially  
562 a bare sclera with the overlying retinal pigmented epithelium, retina or choroid missing (70). It  
563 may be sporadic or inherited and, in some cases, is associated with systemic disorders (70).  
564 Choroidal colobomas in humans can be also associated with the presence of retinal dysplasia  
565 (71, 72), which was noted in the current case. Although there are multiple genetic mutations  
566 associated with colobomatous defects in humans (70), there is only one case report of a  
567 macaque with coloboma and no genetic evaluations were pursued in that report (73). We did not  
568 pursue a genetic evaluation because it seems unlikely that a rare genetic defect would occur in  
569 one of the fetuses with congenital ZIKV infection. The defects in the eye affected the posterior  
570 and ventral aspect of the globe, which is common, since the ocular fissure is embryologically  
571 located in the ventro-nasal quadrant of the eye. It also mainly affected the choroid, thereby  
572 classifying it as a choroidal coloboma. In our previous study, we identified optic nerve gliosis in  
573 the two-first trimester infections (49), but did not identify other significant ocular pathology. CZS  
574 represents a continuum of disease from mild to severe and the macaque model highlights this by  
575 capturing the wide disease spectrum. It is also important to note that the current study was  
576 conducted with a virus stock prepared from an isolate obtained from a person infected in Puerto  
577 Rico, whereas our previous study (49) was conducted with a virus stock prepared from a French  
578 Polynesian isolate. Our results may indicate that closely related viruses can cause different  
579 outcomes in pregnant macaques, however further studies will be needed to understand whether  
580 specific genetic determinants are related to these outcomes. Although ZIKV causes ocular  
581 disease in the adult murine model (74), no ocular anomalies to this extent have yet been  
582 observed in mouse models of congenital ZIKV infection. This also underscores the important role  
583 the rhesus macaque model plays in studying ZIKV effects on pregnancy outcomes.  
584



585 Maternal and fetal tissue viral distribution

586 ZIKV RNA was detected throughout fetal tissues, affecting multiple organ systems (digestive,  
587 respiratory, reproductive, cardiovascular, immune, and nervous), and replication competent virus  
588 was identified in fetal lung tissue 49 dpi via negative and positive strand RNA ISH. Remarkably,  
589 ZIKV RNA was also detected in maternal lymph nodes at 49 dpi and replication competent virus  
590 was identified in the lymph node tested. The presence of vRNA does not imply that the virus is  
591 replicating or may be transmissible. However, the detection of negative strand RNA by ISH and  
592 its colocalization with positive strand vRNA is confirmation of replication competent virus, and the  
593 finding of infectious virus in fetal and maternal tissues 49 dpi could have important implications  
594 for transmission. The fact that replication competent ZIKV is still present in an adult lymphoid-  
595 associated tissue at 49 dpi is critical to understanding the risk involved with organ  
596 transplantation, although with the caveat that viral persistence may be longer in pregnancy. Viral  
597 persistence is not explained by a lack of maternal humoral immune response since the dam  
598 developed neutralizing antibodies at concentrations similar to our previous NHP studies of ZIKV  
599 infections (50, 55).

600

601 We do not know to what extent ZIKV infection of the fetus directly contributed to fetal demise,  
602 since this case is complicated by PPROM with acute chorioamnionitis. Extended exposure of the  
603 fetus to ZIKV is most likely responsible for the ocular pathology observed, and there is no  
604 literature of which we are aware which suggests that bacterial infection results in ocular  
605 malformations. The substantial viral burden in the fetal membranes also supports the hypothesis  
606 that ZIKV contributed to PPROM. The detection of replicating ZIKV intermediates in membranes  
607 and fetal tissues at the time of fetal demise also suggests that active ZIKV infection was ongoing  
608 up until fetal demise.

609

610 In summary, we describe a case of congenital ZIKV infection with severe ocular and  
611 uteroplacental pathology complicated by fetal demise following apparent PPRM. The fetal  
612 ocular pathology recapitulates defects seen in human CZS. This is the first report of an adverse  
613 pregnancy outcome and fetal pathology in an NHP infected with ZIKV strain PRVABC59, and  
614 thus supports the importance of the macaque model for not only defining the risk ZIKV poses for  
615 pregnant women and their fetuses in the Americas, but also for defining the precise pathways by  
616 which ZIKV accesses the fetal compartment, and for testing strategies to intervene in vertical  
617 transmission.

618

### 619 **Literature Cited**

620

- 621 1. Schuler-Faccini L, Ribeiro EM, Feitosa IM, Horovitz DD, Cavalcanti DP, Pessoa A, et al.  
622 Possible Association Between Zika Virus Infection and Microcephaly - Brazil, 2015. MMWR  
623 Morbidity and mortality weekly report. 2016;65(3):59-62.
- 624 2. Rasmussen SA, Jamieson DJ, Honein MA, Petersen LR. Zika Virus and Birth Defects -  
625 Reviewing the Evidence for Causality. The New England journal of medicine. 2016.
- 626 3. van der Linden V, Filho EL, Lins OG, van der Linden A, Aragao Mde F, Brainer-Lima AM,  
627 et al. Congenital Zika syndrome with arthrogryposis: retrospective case series study. BMJ  
628 (Clinical research ed). 2016;354:i3899.
- 629 4. van der Linden V, Pessoa A, Dobyns W, Barkovich AJ, Junior HV, Filho EL, et al.  
630 Description of 13 Infants Born During October 2015-January 2016 With Congenital Zika Virus  
631 Infection Without Microcephaly at Birth - Brazil. MMWR Morbidity and mortality weekly report.  
632 2016;65(47):1343-8.
- 633 5. Honein MA, Dawson AL, Petersen EE, Jones AM, Lee EH, Yazdy MM, et al. Birth  
634 Defects Among Fetuses and Infants of US Women With Evidence of Possible Zika Virus

- 635 Infection During Pregnancy. JAMA : the journal of the American Medical Association.  
636 2017;317(1):59-68.
- 637 6. Russo FB, Jungmann P, Beltrao-Braga PC. Zika infection and the development of  
638 neurological defects. Cellular microbiology. 2017.
- 639 7. Chan JF, Choi GK, Yip CC, Cheng VC, Yuen KY. Zika fever and congenital Zika  
640 syndrome: An unexpected emerging arboviral disease. The Journal of infection. 2016;72(5):507-  
641 24.
- 642 8. Costa F, Sarno M, Khouri R, de Paula Freitas B, Siqueira I, Ribeiro GS, et al. Emergence  
643 of Congenital Zika Syndrome: Viewpoint From the Front Lines. Annals of internal medicine.  
644 2016;164(10):689-91.
- 645 9. Franca GV, Schuler-Faccini L, Oliveira WK, Henriques CM, Carmo EH, Pedi VD, et al.  
646 Congenital Zika virus syndrome in Brazil: a case series of the first 1501 livebirths with complete  
647 investigation. Lancet. 2016.
- 648 10. Moore CA, Staples JE, Dobyns WB, Pessoa A, Ventura CV, Fonseca EB, et al.  
649 Characterizing the Pattern of Anomalies in Congenital Zika Syndrome for Pediatric Clinicians.  
650 JAMA pediatrics. 2016.
- 651 11. Meyer U, Yee BK, Feldon J. The neurodevelopmental impact of prenatal infections at  
652 different times of pregnancy: the earlier the worse? The Neuroscientist : a review journal bringing  
653 neurobiology, neurology and psychiatry. 2007;13(3):241-56.
- 654 12. Ventura CV, Maia M, Travassos SB, Martins TT, Patriota F, Nunes ME, et al. Risk  
655 Factors Associated With the Ophthalmoscopic Findings Identified in Infants With Presumed Zika  
656 Virus Congenital Infection. JAMA ophthalmology. 2016;134(8):912-8.
- 657 13. Zin AA, Tsui I, Rossetto J, Vasconcelos Z, Adachi K, Valderramos S, et al. Screening  
658 Criteria for Ophthalmic Manifestations of Congenital Zika Virus Infection. JAMA pediatrics. 2017.
- 659 14. Agrawal R, Oo HH, Balne PK, Ng L, Tong L, Leo YS. Zika Virus and Eye. Ocular  
660 immunology and inflammation. 2017:1-6.

- 661 15. Ventura CV, Maia M, Bravo-Filho V, Gois AL, Belfort R, Jr. Zika virus in Brazil and  
662 macular atrophy in a child with microcephaly. *Lancet*. 2016;387(10015):228.
- 663 16. Ventura CV, Fernandez MP, Gonzalez IA, Rivera-Hernandez DM, Lopez-Alberola R,  
664 Peinado M, et al. First Travel-Associated Congenital Zika Syndrome in the US: Ocular and  
665 Neurological Findings in the Absence of Microcephaly. *Ophthalmic surgery, lasers & imaging*  
666 *retina*. 2016;47(10):952-5.
- 667 17. Ventura CV, Ventura LO, Bravo-Filho V, Martins TT, Berrocal AM, Gois AL, et al. Optical  
668 Coherence Tomography of Retinal Lesions in Infants With Congenital Zika Syndrome. *JAMA*  
669 *ophthalmology*. 2016;134(12):1420-7.
- 670 18. Ventura CV, Maia M, Ventura BV, Linden VV, Araujo EB, Ramos RC, et al.  
671 Ophthalmological findings in infants with microcephaly and presumable intra-uterus Zika virus  
672 infection. *Arquivos brasileiros de oftalmologia*. 2016;79(1):1-3.
- 673 19. Miranda HA, 2nd, Costa MC, Frazao MA, Simao N, Franchischini S, Moshfeghi DM.  
674 Expanded Spectrum of Congenital Ocular Findings in Microcephaly with Presumed Zika  
675 Infection. *Ophthalmology*. 2016;123(8):1788-94.
- 676 20. Wong CW, Ng SR, Cheung CM, Wong TY, Mathur R. ZIKA-RELATED MACULOPATHY.  
677 *Retinal cases & brief reports*. 2017.
- 678 21. Yepez JB, Murati FA, Pettito M, Penaranda CF, de Yepez J, Maestre G, et al. Ophthalmic  
679 Manifestations of Congenital Zika Syndrome in Colombia and Venezuela. *JAMA ophthalmology*.  
680 2017;135(5):440-5.
- 681 22. Centers for Disease Control and Prevention. Pregnant Women with Any Laboratory  
682 Evidence of Possible Zika Virus Infection in the United States and Territories [updated March 2,  
683 2017. Available from: <https://www.cdc.gov/zika/geo/pregwomen-uscases.html>.
- 684 23. Sarno M, Sacramento GA, Khouri R, do Rosario MS, Costa F, Archanjo G, et al. Zika  
685 Virus Infection and Stillbirths: A Case of Hydrops Fetalis, Hydranencephaly and Fetal Demise.  
686 *PLoS neglected tropical diseases*. 2016;10(2):e0004517.

- 687 24. Schaub B, Monthieux A, Najihoullah F, Harte C, Cesaire R, Jolivet E, et al. Late  
688 miscarriage: another Zika concern? European journal of obstetrics, gynecology, and reproductive  
689 biology. 2016;207:240-1.
- 690 25. van der Eijk AA, van Genderen PJ, Verdijk RM, Reusken CB, Mogling R, van Kampen JJ,  
691 et al. Miscarriage Associated with Zika Virus Infection. The New England journal of medicine.  
692 2016.
- 693 26. Martines RB, Bhatnagar J, Keating MK, Silva-Flannery L, Muehlenbachs A, Gary J, et al.  
694 Notes from the Field: Evidence of Zika Virus Infection in Brain and Placental Tissues from Two  
695 Congenitally Infected Newborns and Two Fetal Losses - Brazil, 2015. MMWR Morbidity and  
696 mortality weekly report. 2016;65(6):159-60.
- 697 27. Morgan TK. Role of the Placenta in Preterm Birth: A Review. American journal of  
698 perinatology. 2016;33(3):258-66.
- 699 28. Kapogiannis BG, Chakhtoura N, Hazra R, Spong CY. Bridging Knowledge Gaps to  
700 Understand How Zika Virus Exposure and Infection Affect Child Development. JAMA pediatrics.  
701 2017;171(5):478-85.
- 702 29. Prevention; CfDCa. Outcomes of Pregnancies with Laboratory Evidence of Possible Zika  
703 Virus Infection in the United States and the US Territories 2017 [Available from:  
704 <https://www.cdc.gov/zika/reporting/pregnancy-outcomes.html>].
- 705 30. Racicot K, Cardenas I, Wunsche V, Aldo P, Guller S, Means RE, et al. Viral infection of  
706 the pregnant cervix predisposes to ascending bacterial infection. Journal of immunology  
707 (Baltimore, Md : 1950). 2013;191(2):934-41.
- 708 31. Carroll T, Lo M, Lanteri M, Dutra J, Zarbock K, Silveira P, et al. Zika virus preferentially  
709 replicates in the female reproductive tract after vaginal inoculation of rhesus macaques. PLoS  
710 pathogens. 2017;13(7):e1006537.

- 711 32. Paz-Bailey G, Rosenberg ES, Doyle K, Munoz-Jordan J, Santiago GA, Klein L, et al.  
712 Persistence of Zika Virus in Body Fluids - Preliminary Report. *The New England journal of*  
713 *medicine*. 2017.
- 714 33. Sotelo JR, Sotelo AB, Sotelo FJB, Doi AM, Pinho JRR, Oliveira RC, et al. Persistence of  
715 Zika Virus in Breast Milk after Infection in Late Stage of Pregnancy. *Emerging infectious*  
716 *diseases*. 2017;23(5):856-7.
- 717 34. Oliveira Souto I, Alejo-Cancho I, Gascon Brustenga J, Peiro Mestres A, Munoz Gutierrez  
718 J, Martinez Yoldi MJ. Persistence of Zika virus in semen 93 days after the onset of symptoms.  
719 *Enfermedades infecciosas y microbiologia clinica*. 2016.
- 720 35. Atkinson B, Thorburn F, Petridou C, Bailey D, Hewson R, Simpson AJ, et al. Presence  
721 and Persistence of Zika Virus RNA in Semen, United Kingdom, 2016. *Emerging infectious*  
722 *diseases*. 2017;23(4):611-5.
- 723 36. Gaskell KM, Houlihan C, Nastouli E, Checkley AM. Persistent Zika Virus Detection in  
724 Semen in a Traveler Returning to the United Kingdom from Brazil, 2016. *Emerging infectious*  
725 *diseases*. 2017;23(1):137-9.
- 726 37. Turmel JM, Abgueguen P, Hubert B, Vandamme YM, Maquart M, Le Guillou-Guillemette  
727 H, et al. Late sexual transmission of Zika virus related to persistence in the semen. *Lancet*.  
728 2016;387(10037):2501.
- 729 38. Hirayama T, Mizuno Y, Takeshita N, Kotaki A, Tajima S, Omatsu T, et al. Detection of  
730 dengue virus genome in urine by real-time reverse transcriptase PCR: a laboratory diagnostic  
731 method useful after disappearance of the genome in serum. *Journal of clinical microbiology*.  
732 2012;50(6):2047-52.
- 733 39. de Laval F, Matheus S, Labrousse T, Enfissi A, Rousset D, Briolant S. Kinetics of Zika  
734 Viral Load in Semen. *The New England journal of medicine*. 2017;377(7):697-9.
- 735 40. Barzon L, Pacenti M, Franchin E, Lavezzo E, Trevisan M, Sgarabotto D, et al. Infection  
736 dynamics in a traveller with persistent shedding of Zika virus RNA in semen for six months after

- 737 returning from Haiti to Italy, January 2016. Euro surveillance : bulletin Europeen sur les maladies  
738 transmissibles = European communicable disease bulletin. 2016;21(32).
- 739 41. Barzon L, Pacenti M, Berto A, Sinigaglia A, Franchin E, Lavezzo E, et al. Isolation of  
740 infectious Zika virus from saliva and prolonged viral RNA shedding in a traveller returning from  
741 the Dominican Republic to Italy, January 2016. Euro surveillance : bulletin Europeen sur les  
742 maladies transmissibles = European communicable disease bulletin. 2016;21(10).
- 743 42. Dupont-Rouzeyrol M, Biron A, O'Connor O, Huguon E, Descloux E. Infectious Zika viral  
744 particles in breastmilk. Lancet. 2016.
- 745 43. Van den Bossche D, Cnops L, Van Esbroeck M. Recovery of dengue virus from urine  
746 samples by real-time RT-PCR. European journal of clinical microbiology & infectious diseases :  
747 official publication of the European Society of Clinical Microbiology. 2015;34(7):1361-7.
- 748 44. de Souza Pereira BB, Darrigo Junior LG, de Mello Costa TC, Felix AC, Simoes BP,  
749 Stracieri AB, et al. Prolonged viremia in dengue virus infection in hematopoietic stem cell  
750 transplant recipients and patients with hematological malignancies. Transplant infectious disease  
751 : an official journal of the Transplantation Society. 2017.
- 752 45. Bandeira AC, Campos GS, Rocha VF, Souza BS, Soares MB, Oliveira AA, et al.  
753 Prolonged shedding of Chikungunya virus in semen and urine: A new perspective for diagnosis  
754 and implications for transmission. IDCases. 2016;6:100-3.
- 755 46. Arragain L, Dupont-Rouzeyrol M, O'Connor O, Sigur N, Grangeon JP, Huguon E, et al.  
756 Vertical Transmission of Dengue Virus in the Peripartum Period and Viral Kinetics in Newborns  
757 and Breast Milk: New Data. Journal of the Pediatric Infectious Diseases Society. 2016.
- 758 47. Hirsch AJ, Smith JL, Haese NN, Broeckel RM, Parkins CJ, Kreklywich C, et al. Zika Virus  
759 infection of rhesus macaques leads to viral persistence in multiple tissues. PLoS pathogens.  
760 2017;13(3):e1006219.
- 761 48. Aid M, Abbink P, Larocca RA, Boyd M, Nityanandam R, Nanayakkara O, et al. Zika Virus  
762 Persistence in the Central Nervous System and Lymph Nodes of Rhesus Monkeys. Cell. 2017.

- 763 49. Nguyen SM, Antony KM, Dudley DM, Kohn S, Simmons HA, Wolfe B, et al. Highly  
764 efficient maternal-fetal Zika virus transmission in pregnant rhesus macaques. *PLoS pathogens*.  
765 2017;13(5):e1006378.
- 766 50. Dudley DM, Aliota MT, Mohr EL, Weiler AM, Lehrer-Brey G, Weisgrau KL, et al. A rhesus  
767 macaque model of Asian-lineage Zika virus infection. *Nature communications*. 2016;7:12204.
- 768 51. Enders AC. Implantation in the macaque: expansion of the implantation site during the  
769 first week of implantation. *Placenta*. 2007;28(8-9):794-802.
- 770 52. Blankenship TN, Enders AC, King BF. Trophoblastic invasion and the development of  
771 uteroplacental arteries in the macaque: immunohistochemical localization of cytokeratins,  
772 desmin, type IV collagen, laminin, and fibronectin. *Cell and tissue research*. 1993;272(2):227-36.
- 773 53. Bondarenko GI, Burleigh DW, Durning M, Breburda EE, Grendell RL, Golos TG. Passive  
774 immunization against the MHC class I molecule Mamu-AG disrupts rhesus placental  
775 development and endometrial responses. *Journal of immunology (Baltimore, Md : 1950)*.  
776 2007;179(12):8042-50.
- 777 54. Osuna CE, Lim SY, Deleage C, Griffin BD, Stein D, Schroeder LT, et al. Zika viral  
778 dynamics and shedding in rhesus and cynomolgus macaques. *Nature medicine*.  
779 2016;22(12):1448-55.
- 780 55. Aliota MT, Dudley DM, Newman CM, Mohr EL, Gellerup DD, Breitbach ME, et al.  
781 Heterologous Protection against Asian Zika Virus Challenge in Rhesus Macaques. *PLoS*  
782 *neglected tropical diseases*. 2016;10(12):e0005168.
- 783 56. Adams Waldorf KM, Stencel-Baerenwald JE, Kapur RP, Studholme C, Boldenow E,  
784 Vornhagen J, et al. Fetal brain lesions after subcutaneous inoculation of Zika virus in a pregnant  
785 nonhuman primate. *Nature medicine*. 2016.
- 786 57. Tarantal AF. *Ultrasound Imaging in Rhesus (Macaca mulatta) and Long-tailed (Macaca*  
787 *fascicularis) Macaques: Reproductive and Research Applications*. *Ultrasound Imaging*: Elsevier  
788 Ltd.; 2005.



- 789 58. Tarantal AF, Hendrickx AG. Characterization of prenatal growth and development in the  
790 crab-eating macaque (*Macaca fascicularis*) by ultrasound. *The Anatomical record*.  
791 1988;222(2):177-84.
- 792 59. Lindsey HS, Calisher CH, Mathews JH. Serum dilution neutralization test for California  
793 group virus identification and serology. *Journal of clinical microbiology*. 1976;4(6):503-10.
- 794 60. Rutanen EM, Pekonen F, Karkkainen T. Measurement of insulin-like growth factor  
795 binding protein-1 in cervical/vaginal secretions: comparison with the ROM-check Membrane  
796 Immunoassay in the diagnosis of ruptured fetal membranes. *Clinica chimica acta; international  
797 journal of clinical chemistry*. 1993;214(1):73-81.
- 798 61. Doyle L, Young CL, Jang SS, Hillier SL. Normal vaginal aerobic and anaerobic bacterial  
799 flora of the rhesus macaque (*Macaca mulatta*). *Journal of medical primatology*. 1991;20(8):409-  
800 13.
- 801 62. Gribnau AA, Geijsberts LG. Morphogenesis of the brain in staged rhesus monkey  
802 embryos. *Advances in anatomy, embryology, and cell biology*. 1985;91:1-69.
- 803 63. Carlson JA, Chen KR. Cutaneous vasculitis update: neutrophilic muscular vessel and  
804 eosinophilic, granulomatous, and lymphocytic vasculitis syndromes. *The American Journal of  
805 dermatopathology*. 2007;29(1):32-43.
- 806 64. Romero R, Miranda J, Chaemsaitong P, Chaiworapongsa T, Kusanovic JP, Dong Z, et  
807 al. Sterile and microbial-associated intra-amniotic inflammation in preterm prelabor rupture of  
808 membranes. *The journal of maternal-fetal & neonatal medicine : the official journal of the  
809 European Association of Perinatal Medicine, the Federation of Asia and Oceania Perinatal  
810 Societies, the International Society of Perinatal Obstet*. 2015;28(12):1394-409.
- 811 65. Aliota MT, Caine EA, Walker EC, Larkin KE, Camacho E, Osorio JE. Characterization of  
812 Lethal Zika Virus Infection in AG129 Mice. *PLoS neglected tropical diseases*.  
813 2016;10(4):e0004682.

- 814 66. Novy MJ, Duffy L, Axthelm MK, Sadowsky DW, Witkin SS, Gravett MG, et al. Ureaplasma  
815 parvum or Mycoplasma hominis as sole pathogens cause chorioamnionitis, preterm delivery, and  
816 fetal pneumonia in rhesus macaques. *Reproductive sciences* (Thousand Oaks, Calif).  
817 2009;16(1):56-70.
- 818 67. Adams Waldorf KM, Rubens CE, Gravett MG. Use of nonhuman primate models to  
819 investigate mechanisms of infection-associated preterm birth. *BJOG : an international journal of*  
820 *obstetrics and gynaecology*. 2011;118(2):136-44.
- 821 68. Churchill A, Booth A. Genetics of aniridia and anterior segment dysgenesis. *The British*  
822 *journal of ophthalmology*. 1996;80(7):669-73.
- 823 69. Reis LM, Semina EV. Genetics of anterior segment dysgenesis disorders. *Current*  
824 *opinion in ophthalmology*. 2011;22(5):314-24.
- 825 70. Gregory-Evans CY, Williams MJ, Halford S, Gregory-Evans K. Ocular coloboma: a  
826 reassessment in the age of molecular neuroscience. *Journal of medical genetics*.  
827 2004;41(12):881-91.
- 828 71. Onwochei BC, Simon JW, Bateman JB, Couture KC, Mir E. Ocular colobomata. *Survey of*  
829 *ophthalmology*. 2000;45(3):175-94.
- 830 72. Yanoff MS, J.W. *Ocular Pathology*. 7th ed: Saunders Elsevier; 2015.
- 831 73. Lin CC, Tso MO, Vygantas CM. Coloboma of optic nerve associated with serous  
832 maculopathy. A clinicopathologic correlative study. *Archives of ophthalmology* (Chicago, Ill :  
833 1960). 1984;102(11):1651-4.
- 834 74. Miner JJ, Sene A, Richner JM, Smith AM, Santeford A, Ban N, et al. Zika Virus Infection  
835 in Mice Causes Panuveitis with Shedding of Virus in Tears. *Cell reports*. 2016;16(12):3208-18.

836

837 **Figure Captions**

838

839 Figure 1. Timeline depicting body fluid sampling and procedures throughout pregnancy. Blood,  
840 urine, saliva, amniotic fluid, and CSF were collected as indicated in the schedule above, and  
841 ultrasounds were performed weekly. The axes are not drawn to scale.

842

843 Figure 2. ZIKV vRNA levels in maternal body fluids. vRNA was measured by quantitative RT-  
844 PCR in plasma, urine, amniotic fluid and CSF. The limit of assay quantification is 100 copies/mL  
845 and the limit of detection is 33 copies/mL.

846

847 Figure 3. Neutralizing antibody titers following ZIKV infection. PRNT titers were measured pre  
848 and post infection. The x-axis represents the reciprocal serum dilution ( $\log_{10}$ ) and the y-axis  
849 represents the percent reduction. The dashed lines indicate 90% and 50% reduction.

850

851 Figure 4. Amniotic fluid (AF) markers confirm rupture of membranes. (A) An AmniSure<sup>®</sup> test,  
852 which measures PAMG-1 protein, was performed on pan urine collection (28 dpi, 45 dpi, 49 dpi)  
853 and AF (28 dpi) from the pregnant animal. Nonpregnant control animal urine and pregnant  
854 animal AF are included as controls. (B) Relative pixel density of the Amnisure<sup>®</sup> test strip test  
855 band and control band. (C) Amniotic fluid protein IGFBP-1 ELISA. Body fluids from the pregnant  
856 animal (pan urine collection 28, 42, 45, 49 dpi and AF 28 dpi), nonpregnant negative control  
857 male and female urine samples, amniotic fluid from a control pregnancy were evaluated for the  
858 presence of IGFBP-1. In Panels B and C, white bars denote body fluids from the experimental  
859 animal and grey bars denote control fluids from other animals in the colony.

860

861 Figure 5. Fetal growth measured by ultrasonography. (A) Head circumference (HC), biparietal  
862 diameter (BPD), and femur length (FL) were measured in weekly ultrasounds. All measurements  
863 are depicted as millimeters (mm). The solid grey lines were derived from reference ranges from  
864 Tarantal et al. 2005 to show the mean (black lines) and one, two, and three standard deviations

865 from the mean (grey lines). The HC, BPD, and FL were then plotted along these reference  
866 ranges to observe any deviations from the mean. Representative images of the HC, BPD, and  
867 FL ultrasounds are located to the right of the respective graph. (B) The pGA is plotted against the  
868 aGA (based on gestational age estimated from breeding and menstrual history). The pGA is  
869 shown separately for each measurement: BPD (triangle), HC (square), and FL (circle).

870

871 Figure 6. Maternal and fetal necropsy images. (A) The uterus was removed in entirety from the  
872 abdominal cavity of the dam using sterile instruments and a syringe was used to aspirate the  
873 purulent fluid from inside the uterine cavity. (B) The fetus was removed from the uterus and was  
874 covered in thick fibrinous material. (C) and (D) Placental discs 1 and 2 were covered in the same  
875 thick fibrinous maternal that covered the fetus.

876

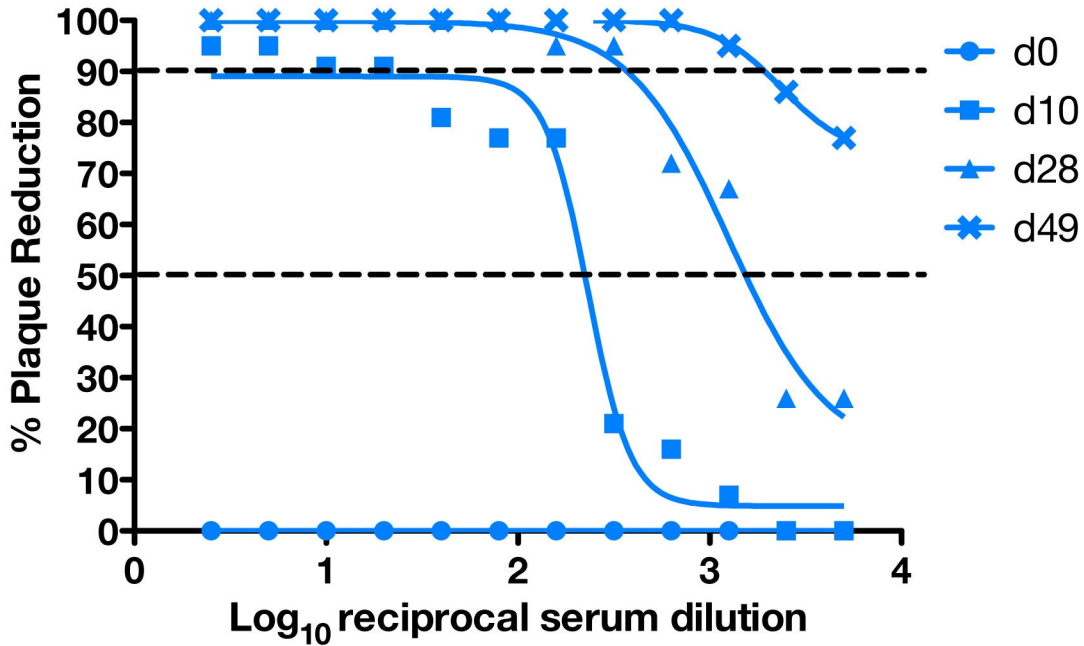
877 Figure 7 Uteroplacental histopathology. (A) Maternal neutrophils invading chorionic plate (arrow)  
878 is diagnostic of acute chorioamnionitis. (B) Villi show increased perivillous fibrin deposition  
879 (arrow) and there are multiple remote infarctions (arrow, C). (D) Radial arteries in the  
880 myometrium show a pronounced leukocytoclastic vasculitis (arrow) defined as an infiltrative  
881 mixture of lymphocytes, eosinophils, and plasma cells into the smooth muscle wall of these  
882 vessels.

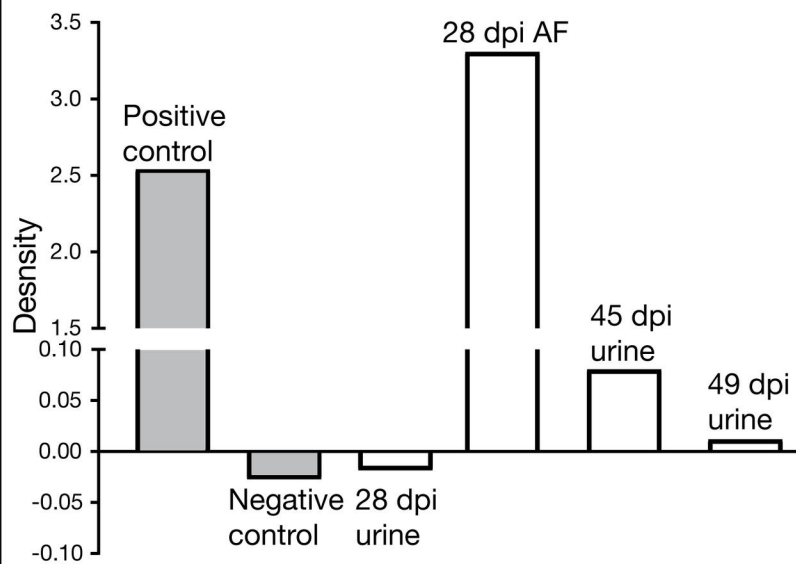
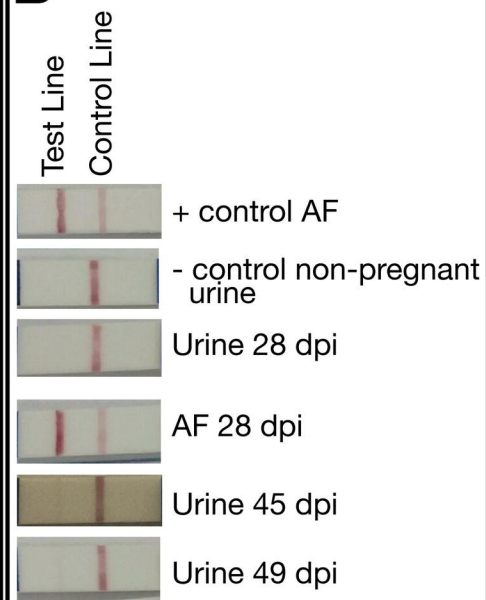
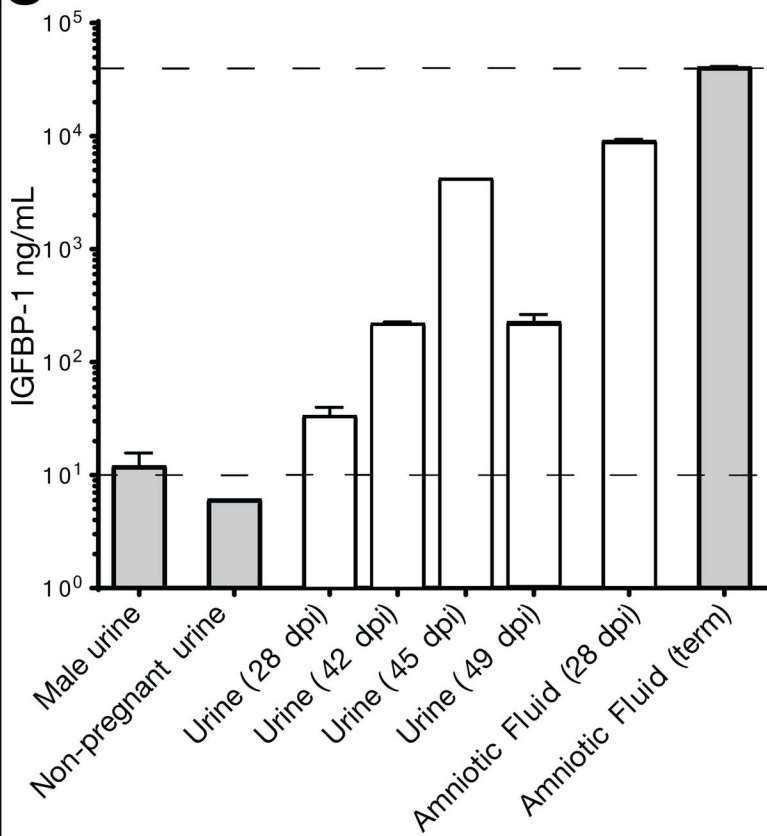
883

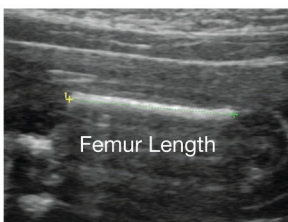
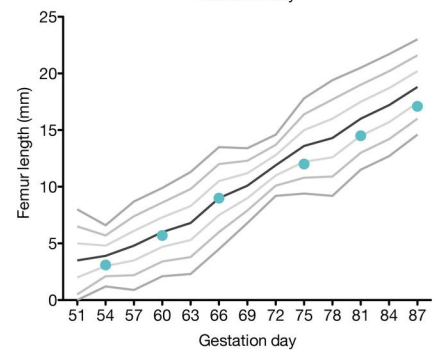
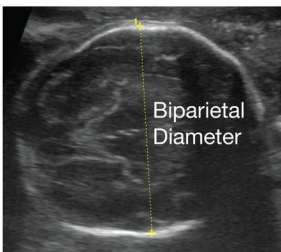
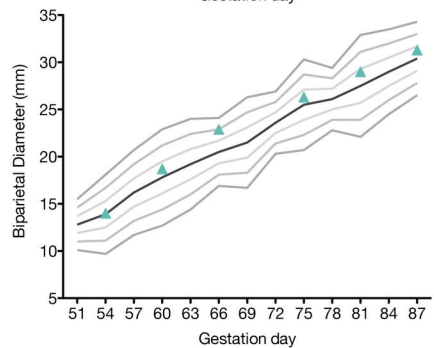
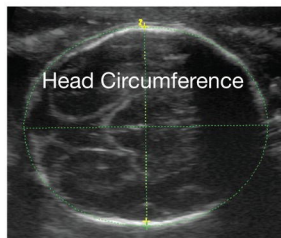
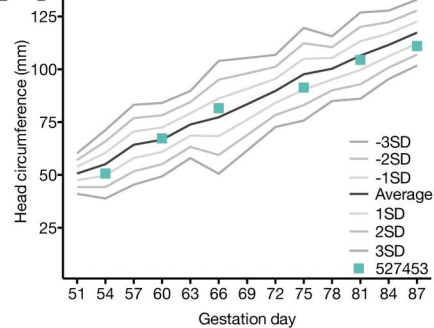
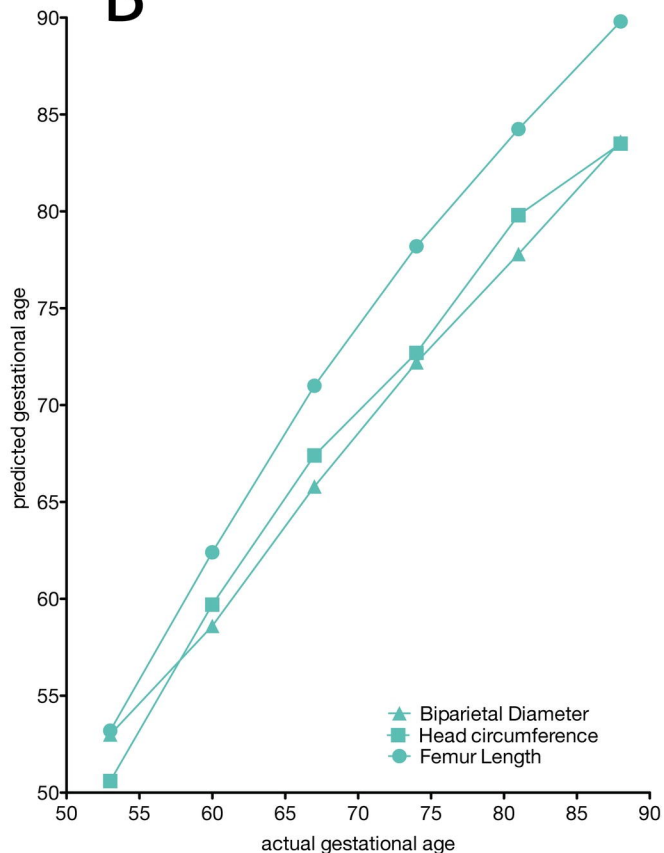
884 Figure 8. Fetal ocular pathology. (A) The left panels contain images of the ZIKV-infected eye,  
885 and the right panels show normal features from a different infant macaque for comparison. The  
886 globe of the ZIKV-infected fetus shows a hypoplastic choroid and dysplastic retina compared to  
887 the normal eye. The irregular shape of the eye in the ZIKV-infected globe is a processing artifact.  
888 The anterior segment image of the ZIKV-infected fetus shows that the iris is fused to the  
889 posterior cornea (black arrow heads), suggesting anterior segment dysgenesis; the dotted line  
890 shows where the iris would be in normal ocular development. The ZIKV-infected eye presents

891 marked retinal dysplasia, characterized by retinal folding and loss of normal retinal organization  
892 when compared with the normal retina in the control image on the right. (B) A choroidal  
893 coloboma was identified on the ventral aspect of the globe (left image); the choroid had normal  
894 development on the dorsal aspect of the same globe (right image). The retina, retinal pigment  
895 epithelium (RPE), choroid (if present), and sclera are labeled with the left image demonstrating  
896 an absence of choroid.

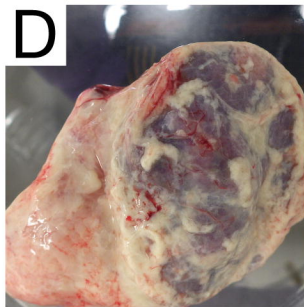
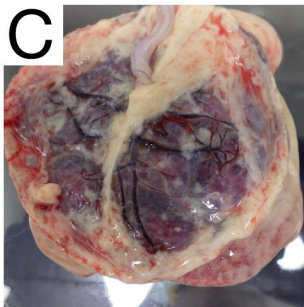
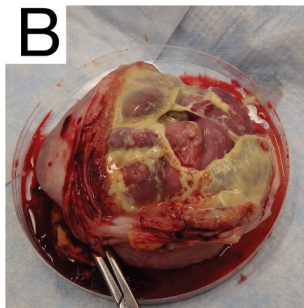
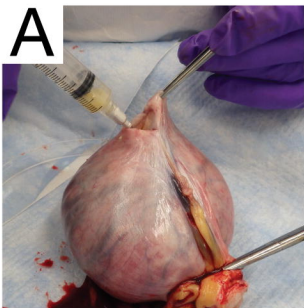
897  
898 Figure 9. Tissue histology and viral localization of maternal spleen, maternal uterus,  
899 amniotic/chorionic membrane, and fetal lung. Each tissue was stained with H&E, ISH, and  
900 mFISH. ISH shows localization of ZIKV vRNA. mFISH shows replicative intermediates by  
901 staining the negative sense RNA strands green and positive sense RNA strands red. Co-  
902 localization (yellow) demonstrates dsRNA intermediates. Black arrows denote a germinal center.  
903 Asterisks indicate neutrophils. Blue arrows highlight green, red, or yellow fluorescence.

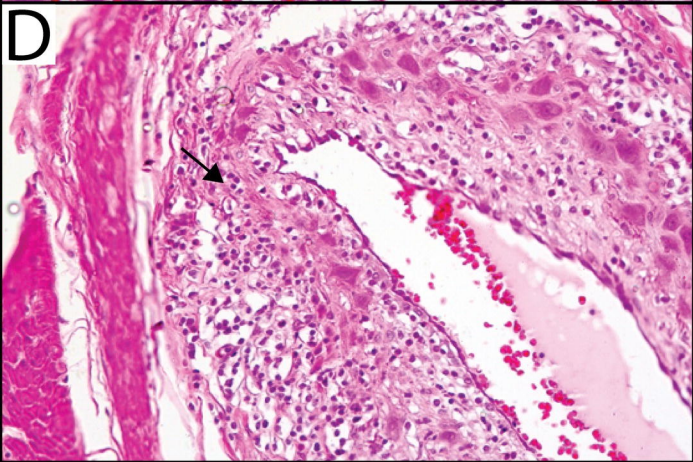
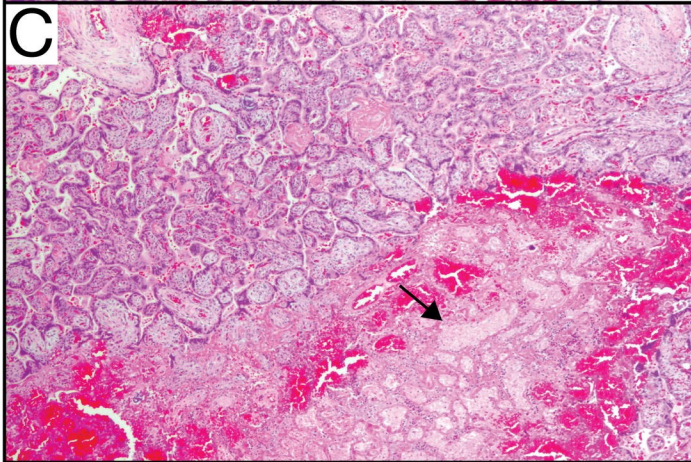
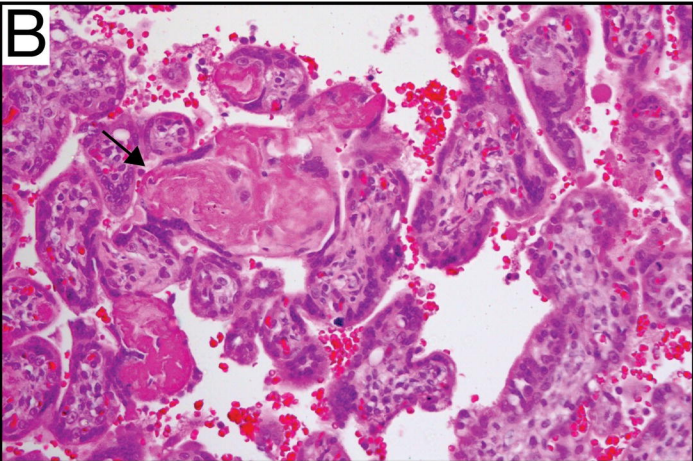
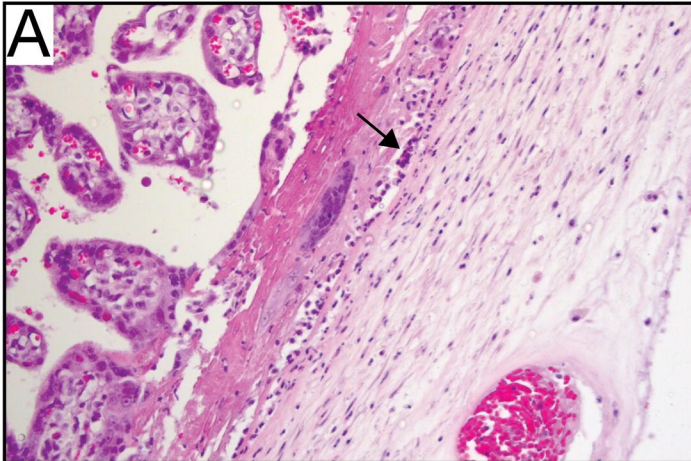


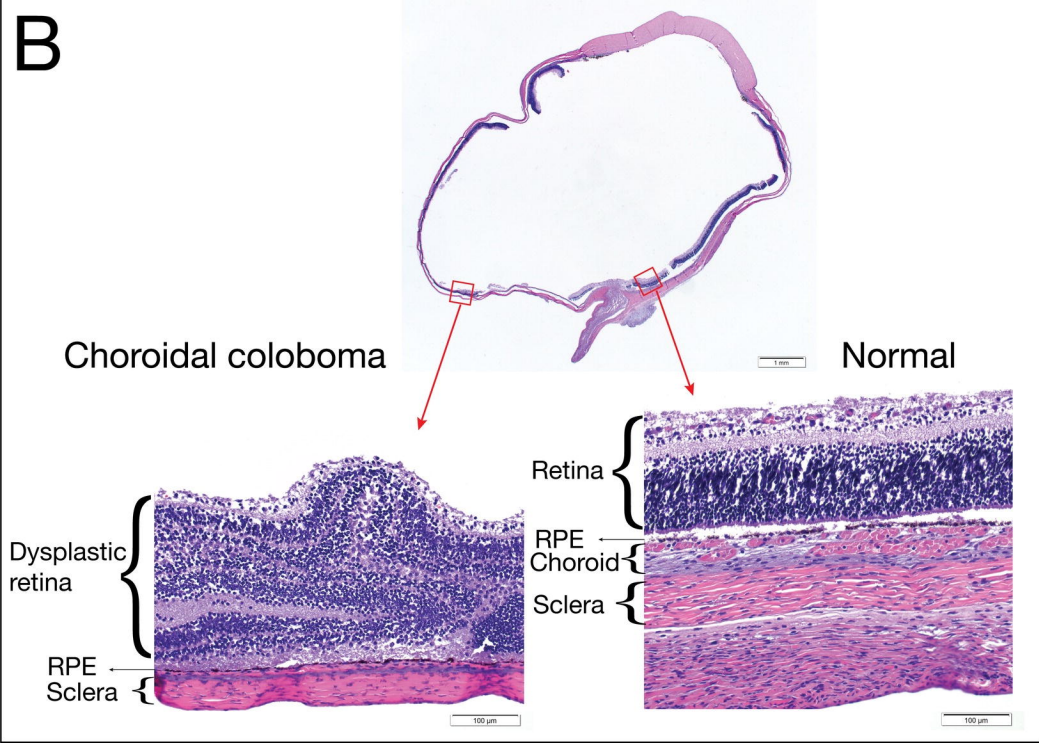
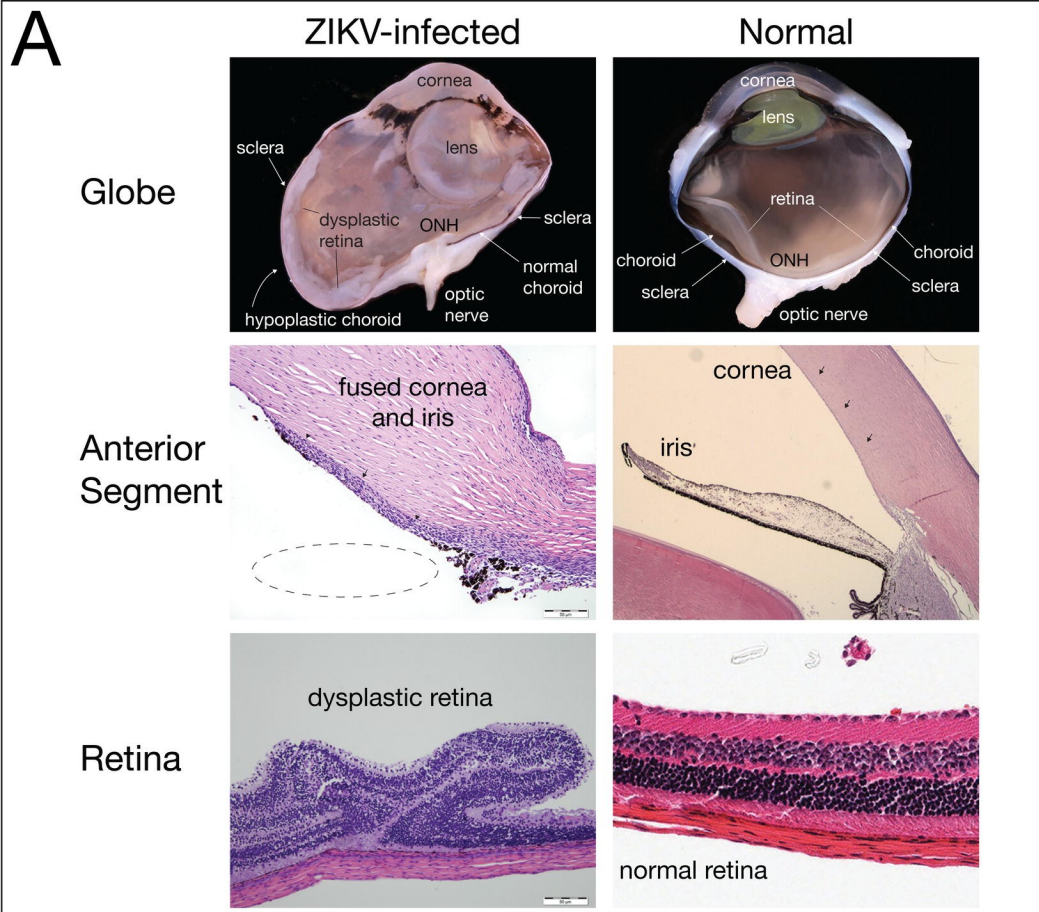
**A****B****C**

**A****B**









H&E

ISH

mFISH

